

PAPER

Single Ag nanoparticle collisions within a dual-electrode micro-gap cell†

Kim McKelvey, *^{ab} Donald A. Robinson, ^a Nicholas J. Vitti,^a Martin A. Edwards ^a and Henry S. White*^a

Received 5th February 2018, Accepted 12th February 2018

DOI: 10.1039/c8fd00014j

An adjustable width (between 600 nm and 20 μm) gap between two Au microelectrodes is used to probe the electrodisolution dynamics of single Ag nanoparticles. One Au microelectrode is used to drive the oxidation and subsequent dissolution of a single Ag nanoparticle, which displays a multi-peak oxidation behavior, while a second Au microelectrode is used to collect the Ag^+ that is produced. Careful analysis of the high temporal resolution current–time traces reveals capacitive coupling between electrodes due to the sudden injection of Ag^+ ions into the gap between the electrodes. The current–time traces allow measurement of the effect of citrate concentration on the electrodisolution dynamics of a single Ag nanoparticle, which reveals that the presence of 2 mM citrate significantly slows down the release of Ag^+ . Intriguingly, these experiments also reveal that only a portion (ca. 50%) of the oxidized Ag nanoparticle is released as free Ag^+ regardless of citrate concentration.

Introduction

Electrochemical monitoring of stochastic nanoparticle–electrode collisions^{1,2} has proved to be a powerful method to study electron transfer in nanoelectrochemical systems,³ to characterize the response of electrocatalytic systems⁴ and to create electrochemical sensors.^{5–7} Of particular interest here is the collision of Ag nanoparticles with an electrode surface, which is held at a sufficiently oxidizing potential to drive the oxidation and subsequent dissolution of the Ag nanoparticle itself.^{8–13} Recently, Ag nanoparticles have been reported to undergo a dynamic multi-peak current–time behavior on a millisecond time scale upon repeated collisions and concurrent partial nanoparticle oxidations at an Au electrode.^{14–16} The multi-peak behavior is the result of the Brownian motion bringing the Ag nanoparticle into and out of contact with the electrode many times to produce multiple peaks in the current–time traces.¹⁷

^aDepartment of Chemistry, University of Utah, Salt Lake City, UT 84112, USA. E-mail: kim.mckelvey@tcd.ie; white@chem.utah.edu

^bSchool of Chemistry, Trinity College Dublin, Dublin 2, Ireland

† Electronic supplementary information (ESI) available. See DOI: 10.1039/c8fd00014j

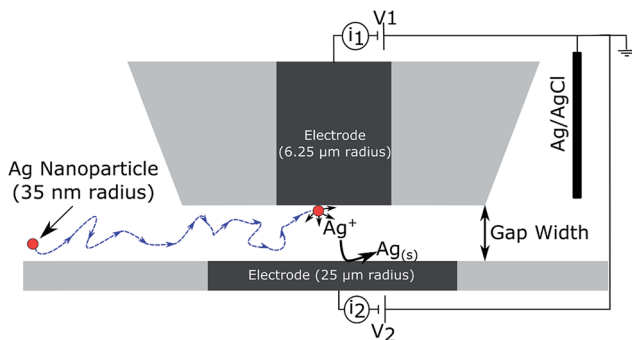


Fig. 1 Schematic of experimental configuration. Two planar-disk Au microelectrodes (a smaller $6.25\ \mu\text{m}$ radius electrode and a larger $25\ \mu\text{m}$ radius electrode) are placed precisely using AC-SECM to form an adjustable micro-gap, with gap widths between $600\ \text{nm}$ and $20\ \mu\text{m}$. A single $35\ \text{nm}$ radius Ag-nanoparticle, which diffuses from the bulk solution, is oxidized at the smaller electrode (held at an oxidizing potential of $V_1 = 750\ \text{mV}$ vs. Ag/AgCl (sat. KCl)) and the Ag^+ that is produced is subsequently reduced (*i.e.*, collected) at the larger electrode (held at a potential V_2). Two currents are measured, the oxidative current at the smaller electrode (i_1) and the reductive current (collection current) at the larger electrode (i_2). Note that the schematic is not drawn to scale.

Here we use a gap between two planar-disk Au microelectrodes to collect Ag^+ ions produced by the oxidation and subsequent electrodisolution of a single Ag nanoparticle, as detailed in Fig. 1. We align precisely the microelectrodes using alternating current scanning electrochemical microscopy (AC-SECM).^{18–20} After alignment and formation of the micro-gap, the $6.25\ \mu\text{m}$ radius Au microelectrode is held at a potential to drive the oxidation of Ag nanoparticles while the larger $25\ \mu\text{m}$ radius Au microelectrode is held at a potential to reduce, and thus collect, Ag^+ . The high temporal resolution (with a $10\ \text{kHz}$ filter) current–time traces of the oxidation and subsequent collection of free Ag^+ allows us to measure the dynamics of Ag nanoparticle electrodisolution and subsequent Ag^+ release with unprecedented resolution.

Kanoufi and Compton previously investigated the dissolution of single Ag nanoparticles upon oxidation on an electrode surface using optical measurements and showed that the dissolution can occur sometime after the oxidation current spike.^{21,22} However, in these previous studies the optical response time was relatively slow at *ca.* $100\ \text{ms}$ and so could only observe the slow dissolution of the Ag nanoparticle after oxidation with additional precipitation agents. In this study we use an electrochemical measurement *via* the dual-electrode micro-gap configuration to monitor the dissolution of the single oxidized nanoparticle with a temporal resolution 1000 folder higher than previous efforts ($0.1\ \text{ms}$ compared to $100\ \text{ms}$).

Experimental

Solutions

Aqueous solutions comprising $20\ \text{mM}$ KNO_3 (Sigma-Aldrich) and $2\ \text{mM}$ trisodium citrate ($\text{Na}_3\text{C}_6\text{H}_5\text{O}_7$, Fisher Scientific), or $20\ \text{mM}$ KNO_3 without added citrate, were prepared using water from a Barnstead Smart2Pure water system (resistivity of

18.2 M Ω cm at 25 °C) on the day of use. Ag nanoparticle solutions were prepared from a stock suspension of 35 nm radius citrate-terminated Ag nanoparticles (AGCB70-1M, Nanocomposix, 1 mg Ag per mL). Note that the Ag nanoparticle solution also contains 2 mM sodium citrate.

Electrode preparation

Two sizes of planar disk-shaped Au microelectrodes were used. The smaller 6.25 μ m radius Au-electrode (CHI105, CH Instruments) was polished to a cone to reduce the glass surrounding the electrode to *ca.* 100 μ m. The larger 25 μ m radius electrode was custom fabricated by sealing a 25 μ m radius Au wire (Goodfellow metals) in a borosilicate capillary and polishing to expose the electrode. Both electrodes were cleaned prior to experiments by polishing on diamond lapping tape (LFCF, Thorlabs) followed by electrochemical cycling between -0.8 V and 1.2 V *vs.* Hg/Hg₂SO₄ (CHI151, CH Instruments) in a 100 mM HClO₄ (Fisher Scientific) solution.

Experimental configuration

The smaller microelectrode was mounted facing vertically downwards as the tip of an electrochemical scanning probe instrument while the larger microelectrode was mounted vertically facing upwards through a Teflon sample holder (see Fig. 1 for schematic of electrode positions). The positions of the two electrodes were controlled by piezoelectric positioners (P753, Physik Instrumente and NPXY-400-132, nPoint) through a FPGA card (PCIe-7852R, National Instruments). The relative electrode positions were controlled, and the position dependent currents recorded at a sampling rate of 13.889 kHz (with a 10 kHz 3-pole Bessel filter on the Dagan current amplifier) using the Warwick Electrochemical Scanning Probe (WEC-SPM) Software.²³

A glass cell was positioned around the Teflon holder. A no-leak Ag/AgCl reference electrode (ET072-1, EDAQ) was inserted into the electrochemical cell. All potentials reported in this work are taken with respect to this sat. KCl reference. Note that the no-leak reference electrode helped prevent Cl⁻ contamination, which we found could interfere with the Ag nanoparticle collision experiments. Two Chem-Clamp (Dagan) current amplifiers were used in parallel to measure the current at each of the electrode, with the reference channel of each amplifier connected to the single Ag/AgCl reference electrode.

Electrode alignment

The two microelectrodes were first coarsely aligned using an optical camera in an unfilled electrochemical cell (see ESI, Section S1[†]). The electrochemical cell was then filled with a solution containing 20 mM KNO₃. A slightly modified version of the Alternating-Current Scanning Electrochemical Microscopy (AC-SECM) technique was used to precisely align the electrodes.²⁰ Briefly, an oscillating potential of 50 mV (RMS) and 9.4 kHz was applied to the 6.25 μ m radius microelectrode (the tip) and a lock-in amplifier (SR830, Stanford Research Systems) used to extract the phase and amplitude of the induced charging current on the second larger 25 μ m radius electrode (the substrate), as shown in the ESI, Section S2.[†] First, a lateral constant-height scan was conducted (a typical scan image is shown in the ESI, Section S3[†]). The lateral position of the electrode was set to the point of maximum

current amplitude on the substrate electrode to precisely align the electrodes laterally. Second, an approach curve was conducted to bring the electrodes close together and create the gap between the electrodes. The point of inflection in the approach curve was used to define the point of closest approach,²⁰ as shown in the ESI, Section S4.† The distance between the two electrodes at the point of closest approach was determined in a separate experiment by monitoring the current for hexaammineruthenium(III) ($\text{Ru}(\text{NH}_3)_6^{3+}$) reduction in negative feedback mode, as shown in the ESI, Section S5.† Finite element simulations were compared to the experimental negative feedback approach curve to determine the distance between the electrodes, *ca.* 600 nm, at the point of closest approach.

Ag nanoparticle oxidation in a micro-gap cell

Once the electrodes were aligned and positioned precisely to create an adjustable gap between the electrodes, the oscillating potential was removed, the solution removed and a solution containing 5×10^9 particles per mL of 35 nm Ag-nanoparticles and either 20 mM KNO_3 and 2 mM trisodium citrate ($\text{Na}_3\text{C}_6\text{H}_5\text{O}_7$), or 20 mM KNO_3 , was very carefully introduced into the electrochemical cell. Current–time traces were recorded (at a sampling rate of 13.889 kHz with a 10 kHz 3-pole Bessel filter on the current amplifier) at a range of gap widths and electrode potentials as specified in the discussion below.

Simulations

Finite element simulations of the transport of Ag^+ across the gap in a 2D axial symmetric geometry was conducted using COMSOL Multiphysics (5.2a, COM-SOL), see ESI, Section S6,† for a full model description.

Results & discussion

In the initial experiments, the smaller (6.25 μm radius) electrode was held at a potential for the oxidation of the Ag nanoparticles (750 mV *vs.* Ag/AgCl (sat. KCl)) and second larger (25 μm radius) electrode was held at a potential to both avoid the reduction of the Ag^+ and oxidation of Ag nanoparticles (*vide infra*, 300 mV *vs.* Ag/AgCl (sat. KCl)), at a gap width of 600 nm. The multi-peak oxidation behavior of an Ag nanoparticle was observed on the oxidation electrode, as shown in Fig. 2A, and has been previously reported by us and others.^{14–17,24} As the multi-peak collisions occur on the oxidation electrode, we observe both small anodic and cathodic currents on the second electrode (Fig. 2B), even though it is held at a potential to avoid reduction of Ag^+ . The average total charge passed during the oxidation of a single nanoparticle is 1.60 ± 0.75 pC; however, the total charge passed on the collection electrode (during the 1 second (by which time the current signal had returned to its baseline) after nanoparticle oxidation) is only 0.09 ± 0.06 pC. The magnitude of the current we observe on the second electrode decreases with an increase in gap width, as shown in the ESI, Section S7,† indicating that the current on the second electrode depends on the distance between the two electrodes. For a single spherical 35 nm radius Ag nanoparticle (Ag density = 10.49 g cm^{-3}) we would expect 1.7 pC for the complete oxidation of a single nanoparticle, in close agreement with what we measure on the oxidation electrode here.

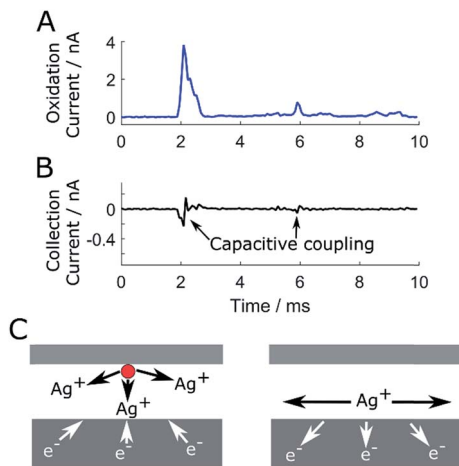


Fig. 2 Capacitive coupling during the electrooxidation of a single Ag-nanoparticle with a gap width of 600 nm. (A) Current–time trace showing the multi-peak oxidation of a single nanoparticle on a 6.25 μm radius Au electrode held at 750 mV vs. Ag/AgCl (sat. KCl). (B) Concurrent current–time trace at the second 25 μm radius Au electrode held at 300 mV vs. Ag/AgCl (sat. KCl) (*i.e.*, a potential where Ag⁺ reduction and Ag nanoparticle oxidation is avoided). (C) Diagram of the capacitive coupling mechanism, with the injection of charge in the form of Ag⁺ (and counter ions, not shown) into the gap leading to an induced capacitance charging of the second electrode.

The anodic and cathodic currents observed on the collection electrode, and the negligible net charge transfer, indicates that these transient currents are due to capacitive charging. As shown in the diagram in Fig. 2, when the Ag nanoparticle is oxidized in the gap a large amount of charge, *i.e.*, Ag⁺ ions, are injected into the gap over a relatively short period of time. As described schematically in the first diagram in Fig. 2C, the first sudden burst of additional charge in the gap at *ca.* 2 ms is immediately compensated by a cathodic capacitive charging current on the collection electrode. Subsequently, as ions from the supporting electrolyte move in the gap to maintain electroneutrality, and as the Ag⁺ ions diffuse in the gap, an anodic transient (at *ca.* 2.1 ms in Fig. 2B) is observed, as shown schematically in the second diagram of Fig. 2C. The capacitive charging current is an inherent feature of nanoparticle collision behavior in micro-gaps that are 1 μm or below in size and occurs in sync with the current–time peaks resulting from Ag nanoparticle electrooxidation.

When both electrodes are held at oxidizing potentials (750 mV vs. Ag/AgCl (sat. KCl)) collision events are only observed on the larger electrode with the 600 nm gap. However, collision events are observed on both electrodes with a very large gap of >20 μm , as shown in the ESI, Section S8.† In a 600 nm gap oxidation events only occur on the larger electrode because of the geometry of the gap. Ag nanoparticles diffuse from the bulk solution into the gap and encounter the larger electrode first, and so are oxidized at this electrode before getting the chance to interact with the smaller electrode. We do, however, still observe variable capacitive coupling on the smaller electrode, as shown in ESI Fig. S8.† Some oxidation events result in strong capacitive coupling while others give rise to weaker coupling, indicating that the distance between the oxidizing nanoparticle and the smaller electrode is variable.

When both electrodes are held at oxidizing potentials (750 mV *vs.* Ag/AgCl (sat. KCl)) and both electrodes are the same size (6.25 μm radius), we observe oxidation events on both electrodes, as is shown in the ESI, Section S9.† According to our previously proposed model, the nanoparticle is allowed to undergo Brownian motion in solution during the time between each electrode collision.¹⁷ Thus, one would expect to observe multipeak current–time behavior at both electrodes for the same nanoparticle if the gap distance is sufficiently small. For example, a Ag nanoparticle may undergo a set of partial oxidation events at electrode 1, then diffuse across the gap to continue undergoing partial oxidations at electrode 2 within roughly 1–100 ms of its departure from electrode 1. However, a single-nanoparticle oxidation event spanning both electrodes was observed only once out of *ca.* 500 individual collision events for this experimental configuration (see the ESI, Section S10†). Due to the experimental configuration, collision events are most likely to occur at the very edge of the electrodes (which are not perfectly aligned) so the probability that a nanoparticle will collide and partially oxidize at both electrodes is presumably lowered.

We now consider collecting Ag^+ ions produced during the oxidation and subsequent dissolution of a single Ag nanoparticle. We oxidize the Ag nanoparticles on a smaller electrode and collect the Ag^+ on a larger electrode to ensure that all the Ag^+ produced is collected, even when the oxidation occurs at the very edge of the smaller electrode. Two typical current–time traces for the oxidation of a single nanoparticle with different collection electrode potentials (–150 mV and 450 mV *vs.* Ag/AgCl (sat. KCl)) are shown in Fig. 3A and C, respectively. Note that a capacitive charging current can also be observed on both traces, although as discussed above the capacitance charge current does not result in any net charge transfer. The cumulative charge for these two events is shown in Fig. 3B and D, respectively. When the collection potential is at –150 mV *vs.* Ag/AgCl (sat. KCl) (Fig. 3A and B), electrooxidation of the nanoparticle at the top electrode results in a sustained reduction current on the collection electrode. However, when the collection electrode is held at 450 mV *vs.* Ag/AgCl (sat. KCl) (Fig. 3C and D) electrooxidation of a nanoparticle at the top electrode results in minimal reduction current on the collection electrode and almost no charge. Fig. 3E shows the collection efficiency (total charge passed by the collection electrode divided by the total charge passed through the oxidation electrode) as a function of collection electrode potential. The sigmoidal response shown in Fig. 3E, with potentials above 250 mV *vs.* Ag/AgCl (sat. KCl) resulting in no collection of Ag^+ and potentials below –100 mV *vs.* Ag/AgCl (sat. KCl) showing a plateau in the collection efficiency, compares to the cyclic voltammogram of $\text{Ag}^{0/+}$ reduction and oxidation shown in Fig. 3F, and indicates that the current at the collection electrode is due to Ag^+ collection.

Interestingly, in Fig. 3E (and Fig. 3B), the collection efficiency plateaus at a value of *ca.* 50%. This indicates that only 50% of the charge that goes into oxidizing an Ag nanoparticle is immediately converted into soluble Ag^+ ions that are collected at the second electrode. One possibility is that Ag^+ ions are escaping out of the gap and therefore are not being collected by the second electrode, which we consider below. Another possibility is that an insoluble irreducible Ag^+ -containing product is being formed. The average oxidation charge of 1.60 ± 0.75 pC per nanoparticle is in agreement with what we expect for complete oxidation of a 35 nm radius Ag nanoparticle and in contrast to the 50% oxidation charge

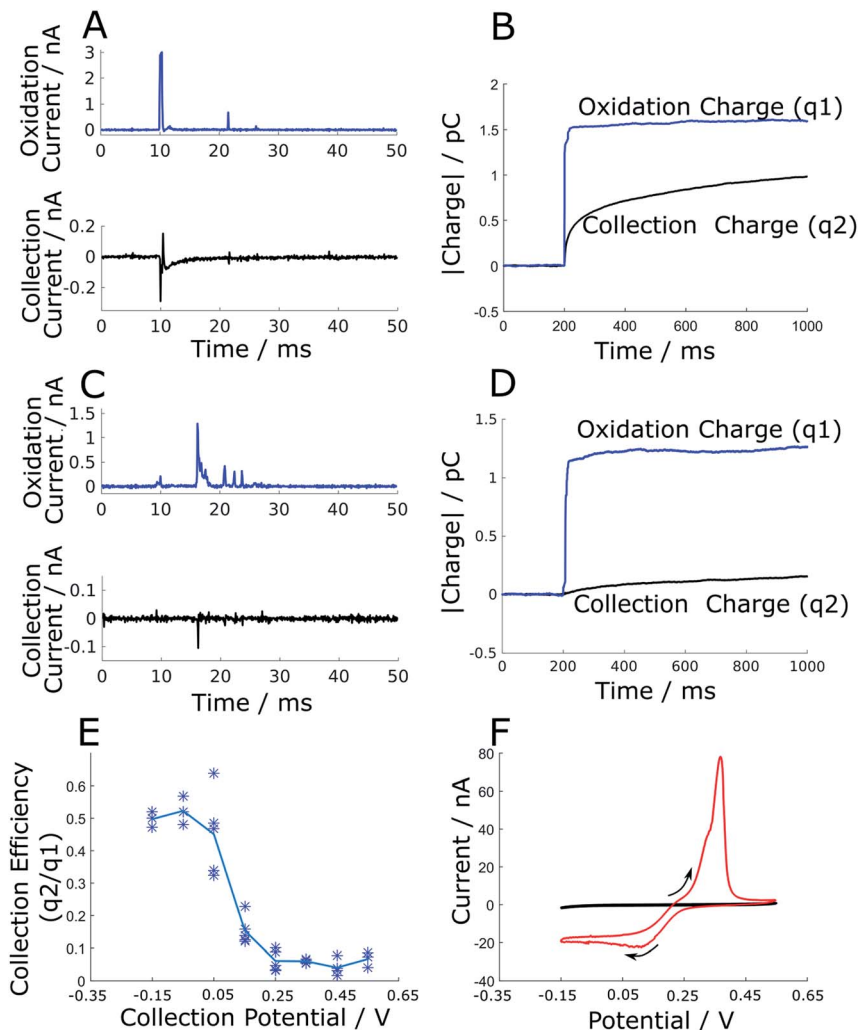


Fig. 3 (A) Current–time traces of a single nanoparticle oxidation and Ag^+ collection with the collection electrode (25 μm radius) held at a potential of -150 mV vs. Ag/AgCl (sat. KCl) and the oxidation electrode (6.25 μm radius) held at 750 mV vs. Ag/AgCl (sat. KCl) in a 600 nm wide gap. (B) Absolute values of the cumulative charge on each electrode for the event in (A). (C) Current–time trace with collection electrode at 450 mV vs. Ag/AgCl (sat. KCl) and the oxidation electrode held at 750 mV vs. Ag/AgCl (sat. KCl). (D) Absolute value of the cumulative charge for each electrode for event in (C). (E) Collection efficiency (q_2/q_1 , over 1 second) as a function of collection potential. (F) Cyclic voltammogram of Ag^+ reduction and oxidation on a 25 μm radius Au microelectrode in 0.5 mM AgNO_3 , 20 mM KNO_3 and 2 mM sodium citrate solution in red, and background in 20 mM KNO_3 and 2 mM sodium citrate solution in black.

previously reported in measurements employing a single microelectrode in bulk solution.^{14–16} In the latter work and others,¹⁷ simulations encompassing the Brownian motion and its oxidation through multiple collisions with the electrode showed that the incomplete oxidation was due to the random thermal motion of the particle taking it away from the electrode surface prior to complete oxidation.

However, in the micro-gap cell, the trajectory of the random walk is restricted by the second electrode (and its sheath), which acts to reflect the Ag nanoparticle back, which due to its potential produces no measurable oxidation current. As the only route for the particle to 'escape' is *via* the narrow gap between the two electrodes, the particle spends longer in the vicinity of the electrode and encounters it on more occasions, leading to a higher probability of complete oxidation (see the ESI, Section S11,† which shows a trend of increasing oxidation charge with decreasing gap width). A similar argument was used to explain the observation that Ag nanoparticle oxidation at nanoband electrodes delivers significantly lower fractional oxidation; however, in contrast, in those experiments the probability of escape was enhanced.²⁴

While holding the potential of the reduction electrode at -150 mV (to ensure we collect the Ag^+ generated), we varied the distance between the electrodes between 600 nm and 20 μm . Typical current–time traces for the oxidation and collection of Ag^+ at two different distances of 600 nm and 16 μm are shown in Fig. 4A and B, respectively. At both distances, collection currents are observed on the reducing electrode, indicating that we are collecting Ag^+ that is produced from single nanoparticle oxidation. Note that the collection current at the larger distance (16 μm) is much smaller in magnitude and occurs over a longer duration compared to the smaller distance (600 nm), as we would expect from the diffusive transport of Ag^+ across the gap. The collection efficiency as a function of gap width is shown in Fig. 4C. As we have seen above, the collection efficiency only ever attains *ca.* 50% even at the closest distance between the two electrodes.

To address the possibility that Ag^+ ions are escaping from the gap, and thus reducing the collection efficiency, we simulated the diffusional transport of Ag^+ from the dissolution of an Ag nanoparticle in different gap widths. The simulated collection efficiency is shown as the blue solid line in Fig. 4C. The simulated response shows that in this gap geometry (a 6.25 μm radius top electrode with 100 μm of surrounding glass and a 25 μm radius bottom electrode) essentially 100% of any Ag^+ generated would be collected at the second electrode at distances less than 10 μm . Even with a much larger electrode spacing of 20 μm , we would expect to see a collection efficiency of 80%, with only 20% of the Ag^+ ions escaping from the gap and avoiding being collected at the reduction electrode. However, this is not what we see experimentally, where we observe only partial collection efficiency, suggesting that an insoluble or poorly soluble Ag^+ product is being formed, possibly a Ag–citrate complex^{25–27} or Ag_2O precipitate.^{28,29} Note that we do not explicitly consider the Brownian motion of the nanoparticle in our finite element simulations, and assume release of Ag^+ ions occurs with the nanoparticle in contact with the oxidizing electrode.

To investigate if an insoluble Ag–citrate complex is reducing the collection efficiency or slowing the release of Ag^+ into solution, we decreased the concentration of sodium citrate in solution from 2 mM to 0.02 mM (the small quantity of sodium citrate arises from the nanoparticle stock solution). A typical single Ag nanoparticle oxidation and collection current–time trace with the reduced sodium citrate concentration of 0.02 mM is shown in Fig. 5. The reduction of citrate concentration increases the peak magnitude of the collection current. This increase in peak current magnitude can be seen when comparing Fig. 5A, which has a collection peak of the same magnitude as the oxidation peak, with Fig. 4A or 3A, which have collection current peaks on the order of 10% the magnitude of the

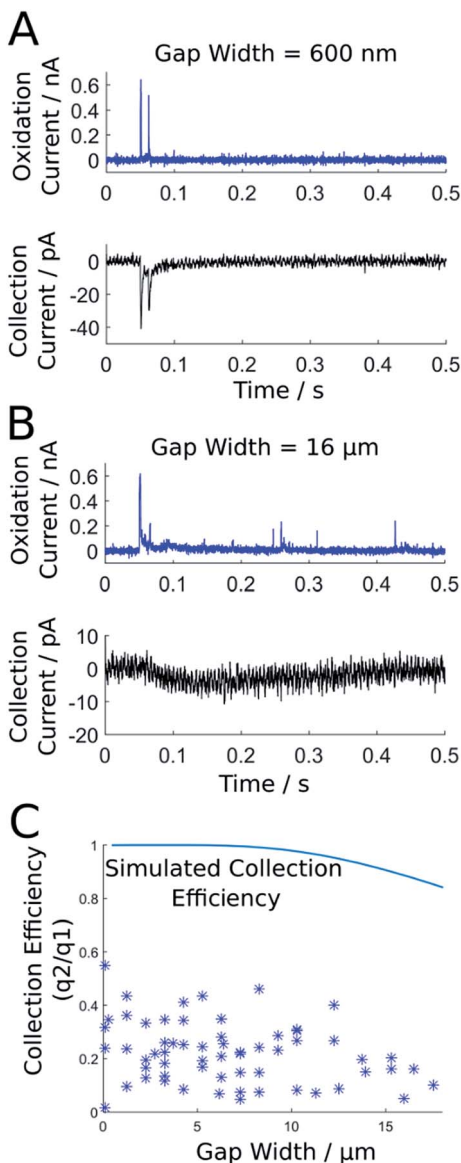


Fig. 4 Oxidation and collection current–time traces with a gap width of 600 nm (A) and 16 μm (B). The oxidation electrode (6.25 μm radius) was held at 750 mV and the collection electrode (25 μm radius) held at -150 mV in a solution of 20 mM KNO_3 and 2 mM sodium citrate. Note the very small capacitive coupling current observed in part B due to the large separation between the electrodes. (C) Collection efficiency as a function of gap width. Also shown is the simulated collection efficiency for the diffusive mass transport of Ag^+ across the gap between the two electrodes assuming instantaneous dissolution of the nanoparticle (see the ESI, Section S6,† for details of simulations).

corresponding oxidation peaks. The decrease in citrate concentration changes the dynamics of Ag^+ release, as shown when comparing the collection charge in Fig. 5B with Fig. 3B. An estimate of the Ag^+ release dynamics can be extracted from

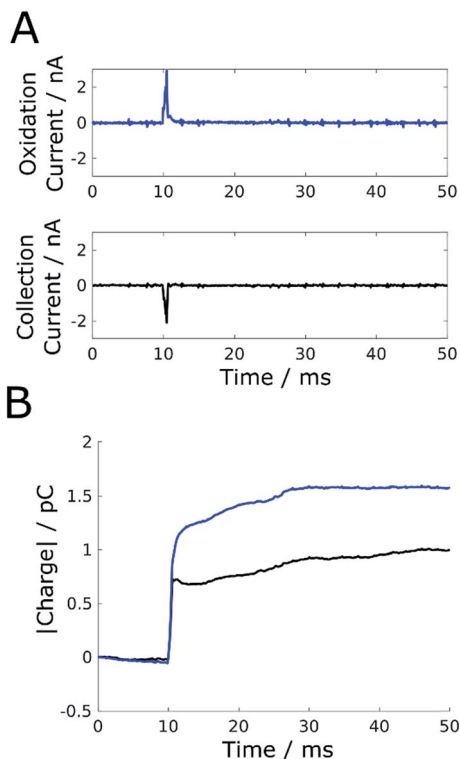


Fig. 5 Typical single Ag nanoparticle oxidation and collection event in 20 mM KNO_3 and 0.02 mM sodium citrate. (A) Current–time traces for the oxidation current (6.25 μm radius Au electrode, 750 mV) and the collection current (25 μm radius Au electrode, -150 mV). (B) Absolute cumulative charge from the oxidation and collection electrodes.

the time to reach half of the maximum charge collected. With 2 mM sodium citrate it takes about 50 ms for the collection charge to reach half of its maximum value (see Fig. 3B), which gives a time constant $\tau \approx 40 \text{ s}^{-1}$, while with 0.02 mM sodium citrate in solution it takes less than 1 ms for the collection charge to reach half the maximum, which gives a time constant $\tau > 1000 \text{ s}^{-1}$. Note that the diffusion coefficient of Ag^+ is $1.6 \times 10^{-5} \text{ cm}^2 \text{ s}^{-1}$ and therefore in a 600 nm gap we would expect the characteristic time for Ag^+ to diffuse across the gap to be $t = L^2/2D = (600 \text{ nm})^2/(2 \times 1.6 \times 10^{-5} \text{ cm}^2 \text{ s}^{-1}) = 0.1 \text{ ms}$. This result shows that the rate of Ag nanoparticle dissolution and Ag^+ release can be mediated by citrate concentration, indicating that an Ag–citrate complex is formed upon nanoparticle oxidation. However, we still obtain a low Ag^+ collection efficiency ($58 \pm 17\%$), which is comparable to measurements performed in solutions containing 2 mM sodium citrate discussed above.

These experiments suggest that the electrooxidation of Ag nanoparticles produces multiple products. When the solution contains an appreciable quantity of citrate (2 mM) a portion of the Ag^+ is rapidly converted to a Ag^+ –citrate complex, which dissolves over 100 ms and is eventually reduced by the collector electrode. However, independent of the citrate concentrations, approx. 50% of the injected charge contributes to a species that is not electrochemically collected at the

collector electrode, either due to its insolubility or because it is not electrochemically reducible. As 50% loss was observed in both 0.02 and 2 mM sodium citrate, the product is unlikely to be a Ag–citrate complex; an Ag oxide species is possible, as was recently observed on a single Ag nanoparticle upon electrooxidation by Zhang,²⁹ and as was recently shown to affect the electrodisolution of single Ag nanoparticles *via* optical dark-field scattering by Willets.²⁸

Conclusions

We have described the electrooxidation of single Ag nanoparticles and the subsequent collection of Ag⁺ generated within an adjustable microscale gap between two working electrodes. At 600 nm gap distances, the sharp bursts of current from Ag nanoparticle oxidation at one electrode give rise to synchronized capacitive bursts of current at the other due to a capacitive coupling response arising from the sudden increase of Ag⁺ concentration within the gap. In addition, the high temporal resolution allows the effect of citrate concentration on the Ag⁺ release upon electrodisolution to be observed, with changes in collection time constant changing from 40 s⁻¹ with 2 mM citrate to >1000 s⁻¹ with 0.02 mM citrate (which approaches the diffusional response time). Finally, we never collect 100% of the charge injected into the electrodisolution of a single nanoparticle as soluble Ag⁺, strongly suggesting that an insoluble Ag⁺ species, most probably Ag₂O, is formed upon electrodisolution of Ag nanoparticles in our experiments.

Conflicts of interest

There are no conflicts to declare.

Acknowledgements

The authors thank Dr Qianjin Chen for electrode fabrication and gratefully acknowledge the support by the Air Force Office of Scientific Research MURI FA9550-14-1-0003.

References

- 1 X. Xiao and A. J. Bard, *J. Am. Chem. Soc.*, 2007, **129**(31), 9610–9612.
- 2 T. J. Anderson and B. Zhang, *Acc. Chem. Res.*, 2016, **49**(11), 2625–2631.
- 3 X. Xiao, S. Pan, J. S. Jang, F. F. Fan and A. J. Bard, *J. Phys. Chem. C*, 2009, **113**(33), 14978–14982.
- 4 L. Zhao, R. Qian, W. Ma, H. Tian and Y. Long, *Anal. Chem.*, 2016, **88**(17), 8375–8379.
- 5 S. V. Sokolov, T. R. Bartlett, P. Fair, S. Fletcher and R. G. Compton, *Anal. Chem.*, 2016, **88**(17), 8908–8912.
- 6 T. M. Alligrant, R. Dasari, K. J. Stevenson and R. M. Crooks, *Langmuir*, 2015, **31**(42), 11724–11733.
- 7 S. J. Kwon and A. J. Bard, *J. Am. Chem. Soc.*, 2012, **134**(26), 10777–10779.
- 8 J. C. Lees, J. Ellison, C. Batchelor-Mcauley, K. Tschulik, C. Damm, D. Omanović and R. G. Compton, *ChemPhysChem*, 2013, **14**(17), 3895–3897.

- 9 J. Ellison, K. Tschulik, E. J. E. Stuart, K. Jurkschat, D. Omanović, M. Uhlemann, A. Crossley and R. G. Compton, *ChemistryOpen*, 2013, **2**(2), 69–75.
- 10 K. Ngamchuea, R. O. D. Clark, S. V. Sokolov, N. P. Young, C. Batchelor-McAuley and R. G. Compton, *Chem.–Eur. J.*, 2017, **23**(63), 16085–16096.
- 11 E. J. E. Stuart, Y.-G. Zhou, N. V. Rees and R. G. Compton, *RSC Adv.*, 2012, **2**(17), 6879–6884.
- 12 N. V. Rees, Y.-G. Zhou and R. G. Compton, *Chem. Phys. Lett.*, 2012, **525–526**, 69–71.
- 13 Y.-G. Zhou, N. V. Rees and R. G. Compton, *Angew. Chem., Int. Ed.*, 2011, **50**(18), 4219–4221.
- 14 S. M. Oja, D. A. Robinson, N. J. Vitti, M. A. Edwards, Y. Liu, H. S. White and B. Zhang, *J. Am. Chem. Soc.*, 2017, **139**(2), 708–718.
- 15 J. Ustarroz, M. Kang, E. Bullions and P. R. Unwin, *Chem. Sci.*, 2017, **8**(3), 1841–1853.
- 16 W. Ma, H. Ma, J.-F. Chen, Y.-Y. Peng, Z.-Y. Yang, H.-F. Wang, Y.-L. Ying, H. Tian and Y.-T. Long, *Chem. Sci.*, 2017, **8**(3), 1854–1861.
- 17 D. A. Robinson, Y. Liu, M. A. Edwards, N. J. Vitti, S. M. Oja, B. Zhang and H. S. White, *J. Am. Chem. Soc.*, 2017, **139**(46), 16923–16931.
- 18 M. A. Alpuche-Aviles and D. O. Wipf, *Anal. Chem.*, 2001, **73**(20), 4873–4881.
- 19 K. Eckhard and W. Schuhmann, *Analyst*, 2008, **133**(11), 1486–1497.
- 20 M. Etienne, A. Schulte and W. Schuhmann, *Electrochem. Commun.*, 2004, **6**(3), 288–293.
- 21 C. Batchelor-McAuley, A. Martinez-Marrades, K. Tschulik, A. N. Patel, C. Combellas, F. Kanoufi, G. Tessier and R. G. Compton, *Chem. Phys. Lett.*, 2014, **597**, 20–25.
- 22 V. Brasiliense, A. N. Patel, A. Martinez-Marrades, J. Shi, Y. Chen, C. Combellas, G. Tessier and F. Kanoufi, *J. Am. Chem. Soc.*, 2016, **138**(10), 3478–3483.
- 23 Warwick Electrochemical Scanning Probe Microscopy, <https://warwick.ac.uk/fac/sci/chemistry/research/unwin/electrochemistry/wec-spm/>, accessed Feb 2, 2018.
- 24 F. Zhang, M. A. Edwards, R. Hao, H. S. White and B. Zhang, *J. Phys. Chem. C*, 2017, **121**(42), 23564–23573.
- 25 S. Djokić, *Bioinorg. Chem. Appl.*, 2008, **2008**, 1–7.
- 26 S. Patra, A. K. Pandey, D. Sen, S. V. Ramagiri, J. R. Bellare, S. Mazumder and A. Goswami, *Langmuir*, 2014, **30**(9), 2460–2469.
- 27 Q. Zhang, Y. Hu, S. Guo, J. Goebel and Y. Yin, *Nano Lett.*, 2010, **10**(12), 5037–5042.
- 28 V. Sundaresan, J. W. Monaghan and K. A. Willets, *J. Phys. Chem. C*, 2018, **122**, 3138.
- 29 R. Hao, Y. Fan and B. Zhang, *J. Am. Chem. Soc.*, 2017, **139**(35), 12274–12282.